NJC

Accepted Manuscript

This is an *Accepted Manuscript*, which has been through the Royal Society of Chemistry peer review process and has been accepted for publication.

Accepted Manuscripts are published online shortly after acceptance, before technical editing, formatting and proof reading. Using this free service, authors can make their results available to the community, in citable form, before we publish the edited article. We will replace this *Accepted Manuscript* with the edited and formatted *Advance Article* as soon as it is available.

You can find more information about *Accepted Manuscripts* in the Information for Authors.

Please note that technical editing may introduce minor changes to the text and/or graphics, which may alter content. The journal's standard Terms & Conditions and the Ethical guidelines still apply. In no event shall the Royal Society of Chemistry be held responsible for any errors or omissions in this *Accepted Manuscript* or any consequences arising from the use of any information it contains.

ROYAL SOCIETY OF CHEMISTRY

www.rsc.org/njc

Journal Name New Journal of Chemistry Dynamic Article Links ►

Cite this: DOI: 10.1039/c0xx00000x

www.rsc.org/xxxxxx

ARTICLE TYPE

Synthesis of tunable ZnS/CuS microspheres and the visible-light photoactivity for rhodamine B

Xuewu Wang,[a] Yanan li,[a] Mingrui Wang,[a] Wenjiang Li,*[a] Minfang Chen,[a] and Yue Zhao[b]

Received (in XXX, XXX) Xth XXXXXXXXX 20XX, Accepted Xth XXXXXXXXX 20XX
DOI: 10.1039/b000000x

The tunable ZnS/CuS microspheres were readily prepared via replacing Zn^{2+} ions of solid ZnS microspheres with Cu^{2+} ions in the aqueous solution under a hydrothermal condition, which were characterized by XRD, SEM, TEM, UV–Vis, PL and XPS techniques. The thickness of CuS shell on the surface of ZnS core can be controlled by changing the ion-exchanging time, which plays an important role for the visible light photodegradation efficiency of Rhodamine B in the aqueous solution. The degradation rate can rapidly reach ca. 72% under the visible light irradiation for 15min and then ca. 98% after 60min using the ZnS/CuS microspheres as the photocatalyst.

1. Introduction

Transition metal sulfides composite have attracted great deal of attention because of their unique physical/chemical properties and widespread potential applications in various fields, such as catalysis, solar cells, sensors, drug delivery, and environmental issues (water pollution and air pollution).[1-5] As an important II-VI group semiconductor, ZnS with a wide bandgap is a well-known photocatalyst, which can rapidly produce electron-hole pairs by photoexcitation and the highly negative potentials of excited electrons. For example, Zhao *et al*.[6] prepared size-selective zinc sulfide hierarchical structures, which can degrade Rhodamine B under UV light irradiation. Wang *et al*.[7] yielded well-dispersed ZnS microspheres with the photocatalytic activity using $ZnSO_4$ and $SC(NH_2)_2$ as main original reactant. Zhang *et al*.[8] synthesized Bi-doped ZnS hollow spheres with enhanced UV and visible-light photocatalytic H_2-production activity via a cation exchange reaction between ZnS hollow spheres and $Bi(NO_3)_3$. However, due to the large band gap energy (Eg=3.66eV), ZnS as a highly active photocatalyst is restricted in ultraviolet light zone. On the other hand, especilly, due to the environment-friendly properties, relatively narrow and adjustable band gap (Eg=1.5-2.0eV), Cu_xS is becoming an important semiconductor, which could be as highly efficient and stable visible-light photocatalyst in the fields of pollutant treatment.[20] However, the rapid recombination of photogenerated electron-hole pairs of Cu_xS restricts the improvement of degradation efficiency as photocatalyst. Thus, in order to overcome the drawback of ZnS and CuS semiconductors, many theoretical calculations and experiments have demonstrated that the coupling of two semiconductors might create interfacial states that induce extra visible-light activity and facilitate the charge transfer across the heterojunctions, effectively improving the separation of photogenerated electron-hole pairs.[9]

Till now, various narrow bandgap semiconductors such as $Cu_xS(1\leqq x\leqq 2)$,[10-11] CdS,[12] CdSe[13] have been combined with ZnS, presenting a visible light photocatalytic activity. For example, spherical ZnO/ZnS core/shell particles,[14] ZnS/ZnO hybrid nanowires,[15] onion-like CdSe/ZnS heteronanocrystals,[16] CdS/ZnS multilayer films,[17] one dimensional $CuInS_2$/ZnS heterostructured nanomaterials[18] and CdS/ZnS/In_2S_3 microspheres.[19] The interfacial charge transfer(IFCT) of the composite semiconductors can effectively improve the charge separation on both semiconductor units by retarding the recombination process of photogenerated electron-hole pairs. Especially, ZnS/CuS composite materials can fully utilize the visible-light activities of UV-active semiconductors by promoting charge separation at the interfaces. So far, many approaches have been designed to prepare ZnS/CuS composite materials, such as template method,[21] aqueous synthesis,[22] and ion exchange synthesis.[10] Generally, the template approach is a more commonly accepted method for constructing and controlling the size and morphology of the products.[23-25] Shi *et al*.[21] yielded a series of MS (shell)/ZnS (core) and MS (M=Pb,Cu) hollow microspheres by using ZnS microspheres as templates, promising applications in the development of photoelectric devices. Zhang *et al*.[11] designed and obtained a novel porous CuS/ZnS nanosheet photocatalysts, exhibiting a visible light photocatalytic H_2-production activity. Adelifard *et al*.[26] prepared CuS/ZnS binary thin films with mixed structures of CuS hexagonal and ZnS cubic structure grown on glass substrate by the spray pyrolysis technique. Yu *et al*.[10] prepared monodisperse CuS/ZnS composite hollow spheres by an ion-exchange reaction in the alcohol solution, presenting a visible light photocatalytic activity for Rhodamine B (RhB). In this case, the facile preparation of well-crystallized and low-toxic ZnS-based photocatalysts with controllable morphology and highly photocatalytic activity is still a challenge.

Here, we prepared tunable core/shell ZnS/CuS microspheres by a simple hydrothermal and cation exchange method using preformed ZnS micospheres as the core template and $CuCl_2$ aqueous solution as precursors, in which Zn^{2+} ions on the ZnS microspheres can be replaced with Cu^{2+} ions in the aqueous solution. In this experiment, tunable ZnS/CuS microspheres and even CuS hollow spheres were readily synthesized by simply

adjusting ion-exchanging time under a hydrothermal condition. Meanwhile, the visible-light photoactivity of the samples was evaluated using the degradation of Rhodamine B (RhB) as a probe. The thickness of CuS shell plays an important role for the visible-light degradation of Rhodamine B in the aqueous solution. The degradation efficiency of RhB using the ZnS/CuS microspheres obtained in 1 h as the catalyst can reach rapidly ca. 72% under the visible light irradiation for 15min and then ca. 98% after 60min. It is believed that the combination of narrow band gap with wide band gap semiconductor enhances their photocatalytic abilities because the heterostructure of ZnS/CuS can timely transfer the photogenerated electron-hole pairs, and rapidly separate the photogenerated electrons and holes, which is the main active species responsible for the photocatalytic degradation of RhB. [27]

2. Experimental Details

Chemicals: Zinc acetate ($Zn(CH_3COO)_2{\cdot}2H_2O$), Sodium thiosulphate ($Na_2S_2O_3{\cdot}5H_2O$), Copper chloride hydrates ($CuCl_2{\cdot}2H_2O$), Macrogol 400（PEG-400，$HO(CH_2CH_2O)_nH$） and ethylalcohol (C_2H_5OH). All chemicals used in this study were analytical-grade and were purchased from Kewei Chemical Reagent Company of Tianjin without further treatment.

2.1 Synthesis

2.1.1 preparation of ZnS microspheres

ZnS microspheres as the core template were primarily synthesized by a simple hydrothermal approach. Firstly, 3 mmol of $Zn(CH_3COO)_2{\cdot}2H_2O$ were dissolved completely in a beaker containing 10mL of deionized water and 4mL PEG solution (Named precursor A), and 3 mmol of $Na_2S_2O_3{\cdot}5H_2O$ were also dissolved completely in a beaker containing 10mL of deionized water and 4mL PEG solution (Named precursor B). Then, the precursor B was added into precursor A drop by drop with vigorous stirring to get a homogeneous mixture solution. Finally, the mixture solution was transferred to a 50 mL Teflon-lined autoclave and heated at 100°C for 10 h. After cooling to room temperature, the white precipitate was separated by centrifugation, washed with deionized water and ethanol alternately for several times, dried at 60°C in air. The pure spherical ZnS powder was obtained.

2.1.2 preparation of ZnS/CuS microspheres

The typical core/shell ZnS/CuS composite microspheres was synthesized as follows: 10 mL of aqueous solution containing 61.2 mg of $CuCl_2{\cdot}2H_2O$ was added into 15 mL of mixture solution containing 35 mg of ZnS spheres with vigorous stirring. The mixture solution was changed to field gray, indicating patial Zn^{2+} ions on the surface of ZnS spheres were replaced by Cu^{2+} ions. The field gray mixture solution was transferred into a 50 mL of Teflon-lined autoclave maintaining at 100 °C for different times. After cooling to room temperature, the black product was collected, washed with deionized water and ethanol, dried at 60 °C in air. The tunable core/shell ZnS/CuS microspheres were prepared via replacing Zn^{2+} ions of ZnS spheres with Cu^{2+} ions, in which the typical samples of core/shell ZnS/CuS microspheres can be obtained by changing the reaction time for 15 minutes, 1h, 2h and 3h, respectively.

2.2 Characterization

The powder X-ray diffraction (XRD) patterns were recorded by a RIGAKU Pro X-ray diffraction (D/Max 2500 PC) in an operating mode of 20 KV and 150 mA equipped with a Cu Kα line as the irradiation source (λ= 1.54056 Å) in the 2θ rang 10°-80°. The morphologies of the particles were observed by field emission scanning electron microscopy (FESEM) (JSM-6700). Room-temperature photoluminescence (RT-PL) measurements were performed on powder samples with a pulsed Xe laser (RF-5301 PC) as the excitation wavelength of 300 nm. TU-1901 ultra-violet-visible light (UV-Vis) spectrophotometer was used to perform the optical measurements of the sample dispersed in ethanol in the wavelength range of 200 ~ 800 nm. The electronic binding energy of the ZnS/CuS microspheres was examined by X-ray photoelectron spectroscopy (XPS) on a PHI-5000 VersaProbe instrument.

2.3 Catalytic activities

The photocatalytic activity of different products is evaluated by the degradation rate of RhB aqueous solution (20mg/L) under visible-light irradiation (Simulate the full spectrum of sunlight: 300 W xenon lamp with a light filter). Detailed procedures of the visible light ptotocatalytic reaction are as follows: for the each catalytic reaction, 40 mL of the mixed solution containing 0.04g of photocatalyst (pure ZnS microsphere, core/shell ZnS/CuS microspheres and CuS hollow microspheres) and rhodamine B (RhB) (20mg/L) was vigorous stirring in a dark room for 30 minutes to ensure the establishment of an adsorption/desorption equilibrium between the catalyst and RhB molecules. Then, the mixture solution was irradiated for different time intervals with visible light of a 300 W xenon lamp. TU-1901 UV-vis spectrophotometer (Beijing, China) was used to monitor the concentration of RhB solution at regular intervals of 15 min. The characteristic absorption of RhB at 550nm was chosen as the monitored parameter for the photocatalytic degradation process. The catalytic decolorization for the concentration of RhB aqueous solution is a pseudo-first-order reaction and the degradation rate of RhB was calculated by the following formula: [10]

$$\text{Degradation (\%)} = (1-C_t/C_0)\times 100\% \quad (1)$$

where C_0 and C_t represent the RhB initial concentration and the final concentration respectively.

3. Results and Discussions

Fig. 1 shows the XRD pattern of samples of the pure ZnS microspheres (Fig.1a) and the tunable core/shell ZnS/CuS samples obtained in 15 minutes (Fig.1b), 1h (Fig.1c), 2h (Fig.1d) and 3h (Fig.1e). The as-formed ZnS spheres are indexed as pure wurtzite-phase ZnS with lattice constants of a=b=3.820 Å and c=24.960 Å (JCPDS 39-1363)[28], no obvious impurity peaks are detected. However, after treating with Cu^{2+} ions solution in the hydrothermal condition, nearly no diffraction peaks of ZnS can be observed, indicating that it is very fast for the exchanging of Cu^{2+} ions and Zn^{2+} ions. Accordingly, the diffraction peaks of CuS are gradually strengthened, showing that more and more ZnS have been replaced by CuS with increasing reaction time as shown in Fig.1b, 1c, and 1d. After treating for 3 hours, from

Fig.1e, we can see that the diffraction peaks of the sample can be assigned to hexagonal covelline-phase CuS with lattice constants of a=3.792 Å and c=16.34 Å, which are in good agreement with the literature values (JCPDS 06-0464).[29]

The SEM image of the smooth ZnS spheres as the core template is showed in Fig. 2a. After adding the Cu^{2+} ions into the suspension of ZnS spheres in the hydrothermal condition for 1h, the surface of the ZnS sample was roughened with a number of hierarchical particles, indicating that the Cu^{2+} ions have diffused into the surface of ZnS spheres and partial ZnS molecules have been converted to CuS cluster as shown in Fig. 2b. Further increasing the hydrothermal treatment for 2h, the hollow spheres with two-layer structure can be clearly observed from the broken sphere as shown in Fig.2c. Moreover, after extending the hydrothermal treatment for 3h, as well as based on the XRD result, we found that the CuS hollow spheres could be obtained and the ZnS core nearly disappeared, meaning most Zn^{2+} ions were exchanged by Cu^{2+}(Fig 2d). The TEM images of the solid ZnS sphere, and ZnS/CuS samples obtained in 1h and 3h are shown in the Supporting Information (Fig. S1). From Fig.S1-a, the surface of the ZnS particle is perfect smooth. However, the rougher particles are formed on the surface of the ZnS/CuS sample obtained in 1h as shown in Fig.S1-b, and the apparent contrast between the inner core and outer shell is clearly observed, indicating the presence of two different kinds of materials from core to shell, consistence with Chung's report.[30] And the hollow structure can be clearly observed from the broken sample obtained in 3h (Fig.S1-c). As well as the energy dispersive spectrometry (EDS) of the samples are shown in the Supporting Information (Fig.S2). The pure ZnS spheres present the signal of S, Zn and Cu elements, in which Cu signal is actually from the copper grid for supporting the sample.(Fig.S2-a). However, for the samples obtained in 1h and 3h, their EDS both present the peak of Cu, S and O element, no any signal of Zn element, indicating that the exchanging rate of Zn^{2+} and Cu^{2+} ions is very quick, and the signal of Zn element has been obstructed by the CuS layer formed(Fig. S2-b), corresponding to the SEM and XRD results. The mechanism of the reaction and the formation of the core/shell and hollow structure are proposed: Cu^{2+} ions can substitute the Zn^{2+} ions of ZnS solid materials because the solubility products of ZnS ($Ksp=2.93\times10^{-25}$) is larger than that of CuS (6.3×10^{-36}) in deionized water, which is the main driving force for the formation of core/shell ZnS/CuS microspheres and CuS hollow spheres.[10]As the solid ZnS spheres are added into the solution containing Cu^{2+} ions, S^{2-} ions and Zn^{2+} ions begin to diffuse outward; Meanwhile, Cu^{2+} ions in the solution diffuse inward through the interface shell, and reacted with S^{2-} ions to form CuS precipitates on the surface of ZnS. Due to the smaller radius of Cu^{2+} ion, the diffusion rate of Cu^{2+} ions is obviously faster than that of S^{2-} ions, resulting in the inward growth of the CuS shell and the finally formation of hollow spheres.

Figure 3 displays the UV-Vis absorption spectra of pure ZnS microspheres and ZnS/CuS microsphrers obtained in 1h and 3h, respectively. As shown in Fig. 3a, the absorption band shorter than ca. 250 nm in the wavelength can be attributed to the intrinsic band-gap absorption of ZnS spheres due to electron transitions from the valence band to the conduction band.[31] Compared with pure ZnS sample, the ZnS/CuS samples obtained in 1h (Fig.3b) and in 3h (Fig.3c) both present a broad absorption band in the visible region (300-800 nm) because of the presence of CuS components, similar to the previous reports.[33] Moreover, with increasing the content of CuS, an enhanced absorption band in the visible light region is clearly observed from the absorption line of the ZnS/CuS samples obtained in 3h (Fig.3c). In addition to the absorption band in the visible light region, a stronger absorption peak around 275nm can be observed from the Fig.3b, which might be because the fewer CuS clusters formed in 1h were coated around ZnS spheres, and the intimate contact between CuS and ZnS is crucial for the interelectron transfer between the two components, resulting in the direct interfacial charge transfer (IFCT) from the VB of ZnS to CuS.[32] Thus, we can see that the sample obtained in 1h has the absorption in the UV-visible-light region from 200 to 800 nm, implying a good sun-light photocatalytic activity. However, the ZnS/CuS sample obtained in 3h only shows the stronger broad absorption in the visible region (ca.400~700 nm) and in near-IR region (ca. 700~800 nm) because the most ZnS components have been exchanged by CuS.[34]

Since PL emission resulted from the recombination of free carriers, the PL can be used to disclose the efficiency of charge carrier trapping, immigration and transfer, and to understand the fate of photogenerated electrons and holes in the semiconductor. Here, the room-temperature (RT) PL spectra of ZnS spheres and ZnS/CuS samples in ethanol suspension by excitation at 300 nm are shown in Fig.4. From Fig. 4a, two typical PL emission bands of the pure ZnS spheres can be seen: a strong UV emission band at 363nm (3.42eV) and a week blue-green band at 470 nm (2.64eV), which are corresponding to the recombination of photoinduced electron-hole pairs, [35] and intrinsic defects in the ZnS microspheres,[7] respectively. Meanwhile, corresponding to the relatively strong and wide absorption bands in visible-light region, all CuS/ZnS samples show no visible-light emission peaks due to the rapid separation restraint for the recombination of the photogenerated electrons and holes pairs caused by the defect photoluminescence. However, due to the recombination of electrons and holes in the surface states, all ZnS/CuS samples present PL peaks at 328 nm.[36] The exchange time of Zn^{2+} and Cu^{2+} in the reaction has some effects for the intensity of PL peaks of CuS/ZnS samples at 328 nm. From Fig.4b-e, we can see that only the ZnS/CuS sample obtained in 1h presents a stronger PL peak (Fig.4c), consistence with its stronger UV-Vis absorption spectrum in Fig.3b, which is relationship with the content of CuS on the surface of ZnS.[37] The too fewer (Fig.4b) or too more (Fig.4d and 4e) content of CuS will result in lower the PL intensities because of the fewer interelectron transfer between the two components.

The elemental compositions and chemical status of CuS/ZnS obtained in 1h were further analyzed by XPS (Fig.5a). The XPS survey spectra indicated the presence of Cu and S as well as C and O, the peaks of O and C come from H_2O, O_2, and CO_2 adsorbed on the surface of the sample and the surface oxidation of CuS. The binding energies of Cu_{2p}, S_{2p} and Zn_{2p} had been calibrated by referencing the C_{1s} (284.8 eV). As shown in Fig. 5b, the two typical peaks at 932 eV and 952.3eV, corresponding to $Cu(Ⅱ)_{2p3/2}$ and $Cu(Ⅱ)_{2p1/2}$, which are essentially identical binding energies for Cu_{2p} orbital in accordance with Cu^{2+}, [38] the

other peaks are attributed to the surface oxidation of CuS to CuO. [39] The binding energy of S_{2p} centers at ca. 162 eV due to the spin-orbit coupling of $S_{2p3/2}$ and $S_{2p1/2}$ with a valence of -2, meanwhile, the susceptibility of CuS toward oxidation leads to formation of $CuSO_4$ on the surface, the peak at around 167.2 eV in Fig. 5c are probably attributed to the S_{2p} of $CuSO_4$ as reported in the literature.[40] However, the peaks of Zn_{2p} are not significantly observed probably due to the relatively thick CuS capping layer shielding the signal of Zn_{2p}(Fig.5d).

In order to investigate the effects of CuS thickness on the surface of ZnS for the photocatalytic activity, the photodegradation of RhB in the solution using the different ZnS/CuS samples as visible light photocatalysts were investigated, as shown in Fig. 6, in which the thickness of CuS shell was growing from tiny particles to the complete CuS shell under the hydrothermal treatment. Compared with the samples obtained in 15 min, 2h and 3h, it is clearly seen that the ZnS/CuS sample obtained in 1h presents the greatest photocatalytic effect (98% in degradation rate in 60min). Both the thinner and the thicker CuS layers result in decreasing the photodegradation rate of RhB in the solution (see Fig.6a and Fig.6c), indicating that the thickness of CuS formed on the surface of the ZnS core plays an important role for the photocatalytic reaction, which actually forms a suitbale heterojunction of ZnS and CuS. Recently, the heterostructure coupled with different semiconductors has attracted great interest because it can significantly reduce the recombination and speed up the separation rate of photogenerated charge carriers, which provides a promising pathway for solving energy supply and environmental pollution problems.[41-43] It is generally accepted that the photogenerated electrons(e^-) and holes(h^+) can transfer to the surface to react with the adsorbed reactants, the migration direction of the photogenerated charge carriers depends on the band edge position of semiconductors. [44-46] The h^+, ·OH and $\cdot O^{2-}$ with high oxidation ability can degrade dyes to intermediates and finally to CO_2 and H_2O. Wang *et al*.[47] uncovered that the super-oxide radical ion $\bullet O_2^-$ and hydroxyl radical •OH are responsible for the degradation of methyl orange (MO) under visible light using poly(3-hexylthiophene)-modified TiO_2 as the photocatalyst. Wu *et al*. [48] presented the increased surface defects caused by the ZnS layer result in trapping more UV light, further improving the degradation rate of methylene blue (MB) under UV irradiation using ZnO/ZnS heterostructures as photocatalyst. Xiong *et al* [49] reported that the formation rates of •OH radicals on anatase TiO_2 and P_{25} were much higher than that of other semiconductors, in which the photogenerated holes in the valence band of TiO_2 could directly react with H_2O/OH^- to produce •OH and lifetime of photo-generated electrons and holes in titania was relatively long.

In order to investigate the optical property of the ZnS/CuS sample, it is of great importance to determine the band edge level of a semiconductor photocatalyst. Generaly, the potentials of the conduction-band (CB) and valence band (VB) edges of ZnS and CuS were estimated by Mulliken electronegativity theory: [50,51]

$$E_{CB} = \chi - E^e - 0.5\,E_g \qquad E^e = 4.5\text{eV} \qquad (2)$$

$$E_{VB} = E_{CB} + E_g \qquad (3)$$

Where E_{CB} is the conduction band edge potential, χ is the electronegativity of the semiconductor, expressed as the geometric mean of the absolute electronegativity of the constituent atoms, which is defined as the arithmetic mean of the atomic electron affinity and the first ionization energy. The χ values of ZnS and CuS are ca. 5.26 eV and 5.27 eV. E^e is the energy of free electrons on the hydrogen scale ca. 4.5 eV. E_g is the band gap of the semiconductor. Acording to the UV-Vis spectra and Kubelka Munk method,[37] we can get the band gaps of ZnS and CuS: the optical absorption near band edge follows the formula $(\alpha h\nu)^n = A(h\nu - E_g)$, where α, h, ν, Eg, and A are the absorption coefficient, Plank constant, light frequency, band gap, and a constant, respectively. The E_g value can be estimated by extrapolating the straight portion of $(\alpha h\nu)^n - (h\nu)$ plot to the $\alpha = 0$ point (see the Supporting Information (Fig. S3 and Fig. S4). Thus, the band gaps of ZnS and CuS are 3.46 eV and 1.55 eV, consistent with the previos reports.[52-54] Thus, according to Mulliken electronegativity equations, the top of the VB and the bottom of the CB of ZnS are calculated to be 3.36 eV and -0.079 eV. Similarly, the VB and CB of the CuS are estimated to be 1.54 eV and -0.01 eV. Here, the enhanced visible light photocatalytic activity of ZnS/CuS samples can be explained: after adding Cu^{2+} ions into the solution of ZnS spheres, many tiny CuS nuclei were produced on the surface of ZnS spheres because that the ZnS molecules were partially replaced by CuS molecules, and the core/shell CuS/ZnS structure was formed. The core/shell structure actually is a heterostructure combined with narrow bandgap of CuS and wide bandgap ZnS. And the same Fermi energy of the heterostructure leads to the conduction band and valence band of CuS shifting to above that of ZnS as follows as shown in the Supporting Information (Schema SI).[55] The close integration between ZnS and CuS is beneficial to timely transfer the photogenerated electron-hole pairs, and rapidly separate the photogenerated electrons and holes owing to different available band gaps, which can enhance the photocatalytic activity.[56,57] Then, the mechanism can be proposed: Under the irradiation of visible-light, CuS is excited, and the electron−hole pairs are produced. The excited electrons on the CB of CuS transfer to the CB of ZnS, and holes to locate on the VB of CuS at the ZnS/CuS interface. Furthermore, the migration of photogenerated electrons and holes could be promoted by the internal electric field.[58,59] Therefore, the increase in the charge separation of the photogenerated electrons and holes allows both of the photogenerated electrons and holes to participate in the overall photocatalytic reaction. Consequently, the photogenerated electrons could react with the oxygen molecule adsorbed on the surface of ZnS/CuS photocatalyst to yield $\bullet O_2^-$. Photogenerated holes react with water molecules to produce •OH. $\bullet O_2^-$, •OH and photogenerated holes degrade the organic pollutants absorbed on the surface of ZnS/CuS.[60] This can also explain why the CuS/ZnS sample obtained in 15 min only decomposed 44% of RhB (Fig.5a), which is due to insufficient quantity of CuS tiny particles on the surface of ZnS spheres. On the other hand, further increasing the content of CuS, excessive CuS clusters will shield the incident light, resulting in preventing generation of photogenerated electrons by ZnS inside and decreasing the photodegradation rate of RhB (Fig. 5c).[61]

In order to further prove the high visible-light photocatalytic property of the CuS/ZnS samples, the photodegradation efficiencies of RhB in the solution using no catalyst, pure ZnS spheres, CuS/ZnS samples as the photocatalyst are shown in

Fig.7. We can see that the concentration of RhB solution show little change under visible light irradiation for 1h if no any catalyst was added(Fig.7d). The pure ZnS spheres with the wide band gap present a lower visible light photocatalytic activity, only 5% of degradation rate is observed in 1h (Fig.7c). The CuS hollow spheres with the narrow band-gap also shows a low degradation rate 35% for RhB in the visible light condition(Fig.7b). However, the degradation efficiency of RhB using the ZnS/CuS sample obtained in 1h rapidly reached ca.72% under the visible light irradiation for 15 min and then ca. 98% after 60 min, indicating that a suitably thickness of CuS shell on the ZnS core is the key for enhancing the visible light photocatalytic performance. The inset in Fig.7 presents the absorption spectra of a RhB aqueous solution exposed to visible light for 60 min in the presence of ZnS/CuS (curve a), hollow CuS (curve b), pure ZnS (curve c) and no any catalyst (curve d). It is reasonable to infer that the conspicuous decline of absorption peak at λ= 550 nm is attributable to the visible light photocatalytic activity of the ZnS/CuS microspheres. This result clearly demonstrates that the good photocatalytic activity of ZnS/CuS microsphrers are associated with the formation of thinner layer of CuS structures, which are expected to exhibit not only a fast motion of charge carriers but also provide efficient transport pathways to reactant and product molecules.[62] The influence of the photocatalyst dosage of ZnS/CuS sample on the degradation of RhB (20mg/L 40mL) for 1 h has also been investigated. The results are presented in the Supporting Information (Fig. S5). It is clearly seen that the RhB removal is raised with increasing the catalyst amount from 0.04 g to 0.06 g. However, further increasing the catalyst amount above 0.06 g results in decreasing the RhB removal efficiency, which is possible due to the light scattering by catalyst particles.

4. Conclusion

In summary, tunable ZnS/CuS composite microsphere and CuS hollow microsphere structures have been readily synthesized via substitution of Zn^{2+} in ZnS microspheres with Cu^{2+} by changing the reacting time of the hydrothermal treatment. The thickness of CuS shell plays an important role for the visible-light photocatalytic activity. The novel high-efficiency visible-light photocatalyst of ZnS/CuS microspheres can be obtained by controlling the thickness of CuS shell on the ZnS core spheres, which can rapidly separate the photogenerated electrons and holes on the different bandgaps. The degradation efficiency of RhB using the ZnS/CuS microspheres as the catalyst can rapidly reach ca. 72% under the visible light irradiation in 15min and then ca. 98% in 60min. The results in this work further confirm that a proper combination of narrow-bandgap and wide-bandgap semiconductors can lead to novel composites with an improved photoelectronic property, which can be expected to get practical application as photocatalysis, solar cells and sensors.

Acknowledgments

This work was financially supported by National Natural Science Foundation of China (No.51071108) and Tianjin important Natural Science Foundation (No.09JCZDJC18500).

Notes and references

[a] *Key Laboratory of Display Materials & Photoelectric Devices, School of Materials Science and Engineering, Tianjin University of Technology, Tianjin 300384, PR China. Fax: 0086-22-60214028; Tel: 0086-22-60214028; E-mail: liwj@tjut.edu.cn*
[b] *Mechanical Materials and Mechatronics School, Faculty of engineering, University of Wollongong, N Wollongong, NSW 2500, Australia. Email: yue@uow.edu.au*

Reference

Reference

1 Z. Q. Liu, W. Y. Huang, Y. M. Zhang and Y. X. Tong, *Cryst EngComm*, 2012, **14**, 8261.
2 Z. J. Ning, H. N. Tian, C. Z. Yuan, Y. Fu, H. Y. Qin, L. C. Sun, H. Agren, *Chem. Commun.*, 2011, **47**, 1536; Z. S. Yang, C. Y. Chen, C. W. Liu, H. T. Chang, *Chem. Commun.*, 2010, **46**, 5485.
3 M. Lee, K. Yong, *Nanotechnology*, 2012, **23**, 194014.
4 S. Panigrahi, D. Basak, *RSC Adv.*, 2012, **2**, 11963; Q. W. Tian, F. R. Jiang, R. J. Zou, Q. Liu, Z. G. Chen, M. F. Zhu, S. P. Yang, J. L. Wang, J. H. Wang, J. Q. Hu, *ACS NANO*, 2011, **12**, 9761.
5 K. Dong, Z. Liu, Z. H. Li, J. S. Ren, X. G. Qu, *Adv. Mater.*, 2013, **10**, 1;
6 Q. R. Zhao, Y. Xie, Z. G. Zhang and X. Bai, *Cryst. Growth Des.*, 2007, **1**, 153.
7 X. J. Wang, F. Q. Wan, K. Han, C. X. Chai and K. Jiang, *Mater. Charact.*, 2008, **59**, 1765.
8 J. Zhang, S. W. Liu, J. G. Yu and M. Jaroniec, *J. Mater. Chem.*, 2011, **21**, 14655.
9 S. W. Cao, Z. Yin, J. Barber, Freddy Y. C. Boey, S. C. J. Loo and C. Xue, *ACS Appl. Mater. Interfaces,* 2012, **4**, 418.; J. Lahiri and M. Batzill, *J. Phys. Chem. C*, 2008, 112,4304.
10 J. G. Yu, J. Zhang, S. W. Liu, *J. Phys. Chem. C*, 2010, **114**, 13642.
11 J. Zhang, J. G. Yu, Y. M. Zhang, Q. Li, J. R. Gong, *Nano Lett.*,2011, **11**,4774.
12 S. Y. Lu, M. L. Wu, H. L. Cnen, *J. Appl. Phys.*, 2003, **9**, 5789.
13 S. Nizamoglu, H. V. Demir, *OPT EXPRESS*, 2008, **6**, 3515.
14 W. J. Li, G. Song, F. Xie, M. F. Chen, Y. Zhao, *Mater. Lett.*, 2013, **96**, 221;
15 Z. Wang, S. W. Cao, S. C. J. Loo, C. Xue, *CrystEngComm*, 2013, **15**, 5688.
16 H. V. Demir, S. Nizamoglu, E. Mutlugun, T. Ozel, S. Sampra, N. Gaponik, A. Eychmuller, *Nanotechnology,* 2008, **19**, 1.
17 I. O. Oladeji, L. Chow, *Thin Solid Films,* 2005, **474**, 77.
18 L. X. Yi, Y. Y. Liu ,N. L. Yang, Z. Y. Tang, H. J. Zhao. G. H. Ma, Z. G. Su, D. Wang, *Energy Environ. Sci.,* 2013, **6**, 835.
19 Z. Y. Shen, G. Chen, Q. Wang, Y. G. Yu, C. Zhou, Y. Wang, *Nanoscale,* 2012, **4**, 2010.
20 M. Basu, A.K. Sinha, M. Pradhan, S. Sarkar, Y. C. Negishi, Govind, T. Pal, *Environ. Sci. Technol.*, 2010, **44**, 6314.
21 Y. H. Shi, J. Chen, P. W. Shen, *J. Alloys Compd.*, 2007, **441**, 337.
22 C. Corrado, M. Hawker, G. Livingston, S. Medling, F. Bridges, J. Z. Zhang, *Nanoscale*, 2010, **2**, 1213.
23 S. Mann, Angew. *Chem. Int. Ed.*, 2000, **39**, 3392.
24 W. L. Murphy, D. J. Mooney, *J. Am. Chem. Soc.*, 2002, **124**,1910.
25 X. Wu, K. W. Li, H. Wang., *J. Hazard. Mater.*, 2010, **174**, 573.
26 M. Adelifard, H. Eshghi, M. Mehdi Bagheri Mohagheghi, *Opt. Commun.*, 2012, **285**, 4400.
27 G. Z. Shen, D. Chen, C. J. Lee., *J Chem Phys B*, 2006, **110**, 15689; X. R. Zheng, Z. G. Jin, H. L, Y. Q. Wang, X. Wang, H. Y. Du, *Synth. Met.*, 2013, **169**, 25.

28 X. H. Zhong, S. H. Liu , Z. H. Zhang, L. Li, Z. Wei, W. Knoll, *J. Mater. Chem.,* 2004, **14**, 2790.
29 Y. B. Chen, L. Chen, L. M. Wu, *Cryst. Growth Des.,* 2008, **8**, 2736.
30 J. Chung, J. Myoung, J. Oh, S. Lim, *J Phys Chem C,* 2010, **114**, 21360.
31 X. X. Yu, J. G. Yu, B. Cheng and B. B. Huang, Chem. Eur. J., 2009, **15**, 6731; Y. Zhang, Y. D. Li, *J. Phys. Chem. B*, 2004, **108**, 17805.
32 N. Serpone, D. Lawless, R. Khairutdinov, *J. Phys. Chem.*, 1995, **99**, 16646.
33 T. Arai, S. I. Senda, Y. Sato, H. Takahashi, K. Shinoda, B. Jeyadevan, K. Tohji, *Chem. Mater.*, 2008, **20**, 1997.
34 X. O. Qiu, M. Miyauchi, H. G. Yu, H. Irie and K. Hashimoto, *J. Am. Chem. Soc.*, 2010, **132**, 15259.; M. Liu, X. Q. Qiu, M. Miyauchi and K. Hashimoto, *Chem. Mater.*, 2011, **23**, 5282.
35 X. T. Zhang, M. L. Chen, J. Wen, L. L. Wu, H. Gao, D. Zhang, *CrystEngComm*, 2013, **15**, 1908; W. S. Chae, J. H. Yoon, H. Yu, D. J. Jang. Y. R. Kim, *J. Phys. Chem. B*, 2004, **108**, 11509.
36 J. Z. Xu, S. Xu, J. F. Geng, G. X. Li, J. J. Zhu, *Ultrason. Sonochem.* 2006, **13**, 451.
37 N. Serpone, D. Lawless, R. Khairutdinov, *J. Phys. Chem.*, 1995, **99**, 16646.
38 P. Roy, K. Mondal, S. K. Srivastava, *J. Cryst.Growth*, 2008, **8**, 1530.
39 J. P. Espinos, J. Morales, A. Barranco, A. Caballero, J. P. Holgado, A. R. Gonza lez-Elipe, *J. Phys. Chem. B*, 2002, **106**, 6921; J. Morales, J. P. Espinos, A. Caballero, A. R. Gonzalez-Elipe, *J. Phys. Chem. B*, 2005, **109**, 7758.
40 U. T. D. Thuy, N. Q. Liem, C. Parlett, G. Lalev, K. Wilson, *Catal. Commun.*, 2014, **44**, 62.
41 X. B. Chen, S. H. Shen, L. J. Guo, S. S. Mao, *Chem. Rev.* 2010, **110**, 6503.
42 X.Wei, T. F. Xie, L. L. Peng, W. Fu, J. S. Chen, Q. Gao, G. Y. Hong, D. J. Wang, *J. Phys. Chem. C* 2011, **115**, 8637.
43 M. L. Guan, D. K. Ma, S. W. Hu, Y. J. Chen, S. M. Huang, *Inorg. Chem.* 2011, **50**, 800.
44 Y. Hu, D. Z. Li, Y. Zheng, W. Chen, Y. H. He, Y. Shao, X. Z. Fu, G. C. Xiao, *Appl. Catal. B* 2011, **104**, 30.
45 C. S. Guo, M. Ge, L. Liu, G. D. Gao, Y. C. Feng, Y. Q. Wang, *Environ. Sci. Technol*. 2010, **44**, 419.
46 C. Y. Wang, H. Zhang, F. Li, L. Y. Zhu, *Environ. Sci. Technol.* 2010, **44**, 6843.
47 D. S. Wang, J. Zhang, Q. Z. Luo, X. Y. Li, Y. D. Duan, J. An, *J. Hazard. Mater.,* 2009, **169**, 546. J. G. Yu, J. J. Fan, K. L. Lv, *Nanoscale*, 2010, **2**, 2144.
48 D. P. Wu, Y. Jiang, Y. F. Yuan, J. S. Wu, K. Jiang, *J Nanopart Res,* 2011, **13**, 2875.
49 Q. J. Xiang, J. G. Yu, P.K. Wong, *J. Colloid and Interface Science* 2011, **357**, 163.
50 S. Trasatti, *Pure and Applied Chemistry* 1986, 58, 955-966;
51 Y. Xu, M. A. A. Schoonen, *Am. Mineral.* 2008, **5**, 543.
52 Y. Wan, C. Y. Wu, Y. L. Min, S. H. Yu, *Langmuir* 2007, **23**, 8526.
53 H. L. Xu, W. Z. Wang, W. Zhu, L. Zhou, *Nanotechnology* 2006, **17**, 3649.
54 G. X. Chen, M. T. Niu, L. F. Cui, F. Bao, L. H. Zhou, Y. S. Wang, *J. Phys. Chem. C* 2009, **113**, 7522.
55 Y. Wang, Y. R. Su, L. Qiao, L. X. Liu, Q. Su, C. Q. Zhu, X. Q. Liu, *Nanotechnology* 2011, 22 225702; M. Grtzel *Nature* 2001, **414**, 338.
56 X. Zong, H. J. Yan, G. P. Wu, G. J. Ma, F. Y. Wen, L. Wang, C. Li, *J. Am. Chem. Soc.,* 2008, **130**, 7176.
57 K. Maeda, A. K. Xiong, T. Yoshinaga, T. Ikeda, N. Sakamoto, T. Hisatomi, M. Takashima, D. L. Lu, M. Kanehara, T. Setoyama, T. Teranishi, K. Domen, *Angew. Chem. Int. Ed.*, 2010, **49**, 4096.
58 H. G. Kim, P. H. Borse, J. S. Jang, E. D. Jeong, O. S. Jung, Y. J. Suhd, J. S. Lee, *Chem. Commun*. 2009, **5889**.
59 Y. H. Zheng, L. R. Zheng, Y. Y. Zhan, X. Y. Lin, Q. Zheng, K. M. Wei, *Inorg. Chem.* 2007, **46**, 6980.
60 S. Balachandran, M. Swaminathan, *J. Phys. Chem. C* 2012, **116,** 26306.
61 J. G. Yu, T. T. Ma, S. W. Liu, *Phys. Chem. Chem. Phys.*, 2011, **13**, 3491; J. G. Yu, T. T. Ma, G. Liu and B. Cheng, *Dalton Trans*, 2011, **40**, 6635. J. G. Yu, J. J. Fan, K. L. Lv, *Nanoscale*, 2010, **2**, 2144.
62 Q. J. Xiang, K. L. Lv, J. G. Yu, *Appl. Catal. B*, 2010, **96**, 57.

Figure Captions

Fig. 1 XRD pattern of pure ZnS spheres (a); ZnS/CuS samples obtained in 15 minutes (b), 1h (c), 2h (d) and 3h (e).

Fig. 2 SEM image of spheres solid ZnS (a); core/shell ZnS/CuS (b), multilayer ZnS/CuS (c) and hollow CuS (d).

Fig. 3 UV-Vis absorption spectra of as-prepared ZnS spheres (a); ZnS/CuS samples obtained in: 1h (b) and 3h (c).

Fig. 4 PL spectra of as-prepared ZnS spheres (a); the ZnS/CuS samples obtained in: 15min (b), 1h(c), 2h (d) and 3h (e).

Fig. 5 Typical XPS spectra of CuS/ZnS obtained in 1h: survey spectra (a); Cu_{2p} region (b), S_{2p} region (c) and Zn_{2p} region (d).

Fig. 6 Comparison of phtotocatalytic activities of ZnS/CuS samples obtained in: 15min(a), 1h (b), 2h (c) and 3h (d).

Fig. 7 Visible light phtotocatalytic activities for the RhB of: ZnS/CuS samples obtained in 1h (a), ZnS/CuS samples obtained 3h (b), pure ZnS sample (c) and RhB solution (d).

Graphical abstract

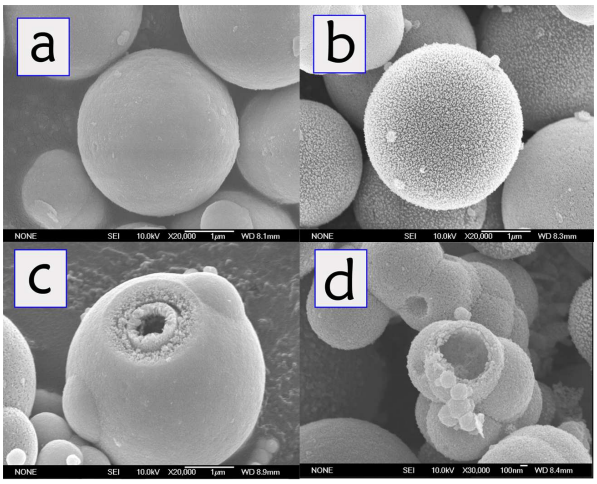

Highlight

The heterostructure of ZnS/CuS obtianed can timely transfer and separate the photogenerated electrons and holes, which enhances their photocatalytic abilities.

Figures

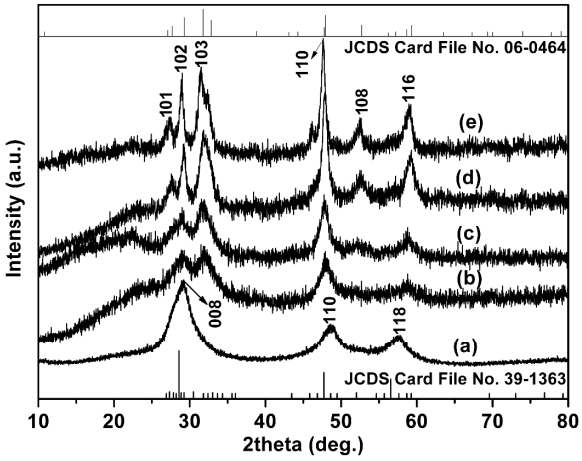

Figure 1

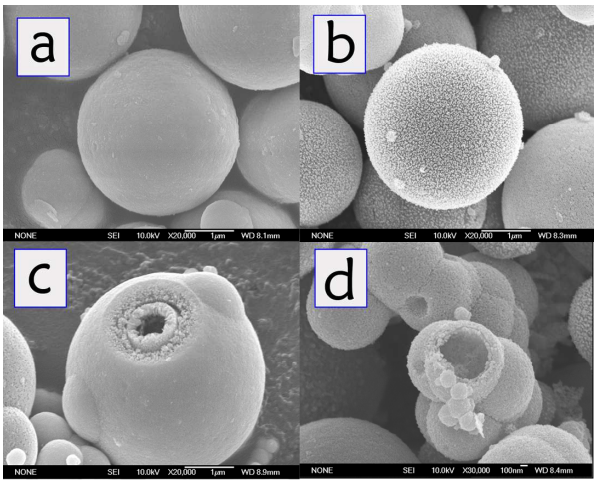

Figure 2

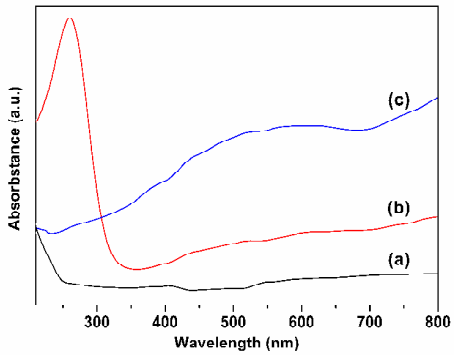

Figure 3

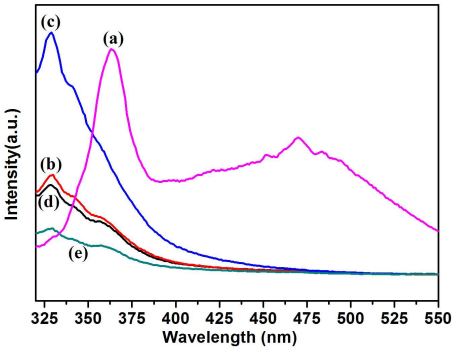

Figure 4

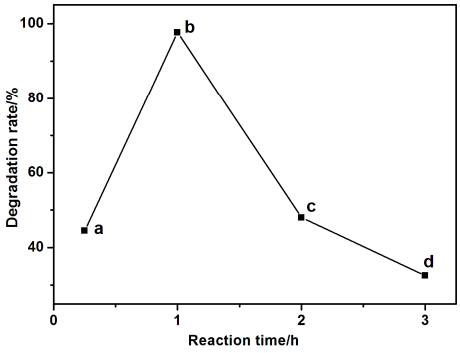

Figure 5

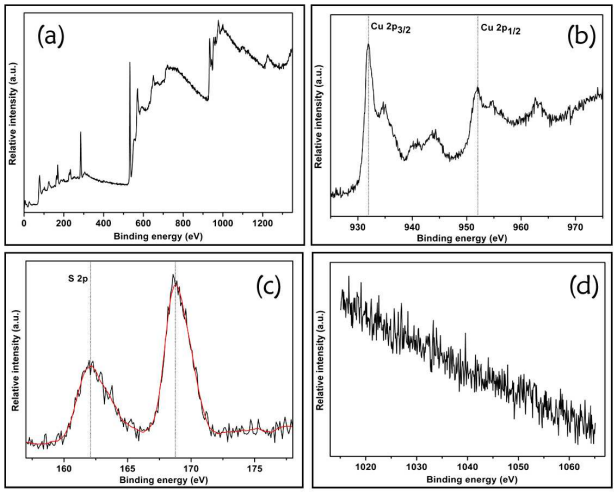

Figure 6

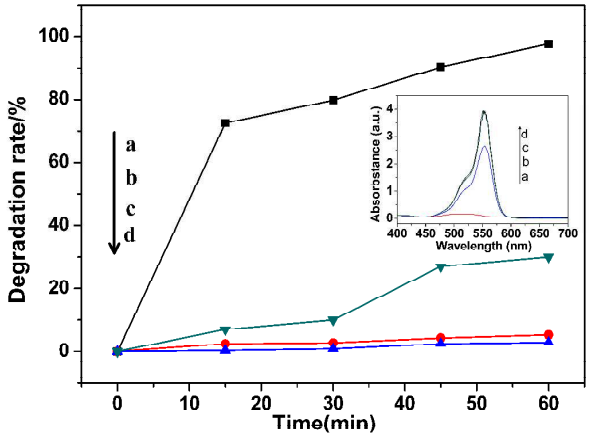

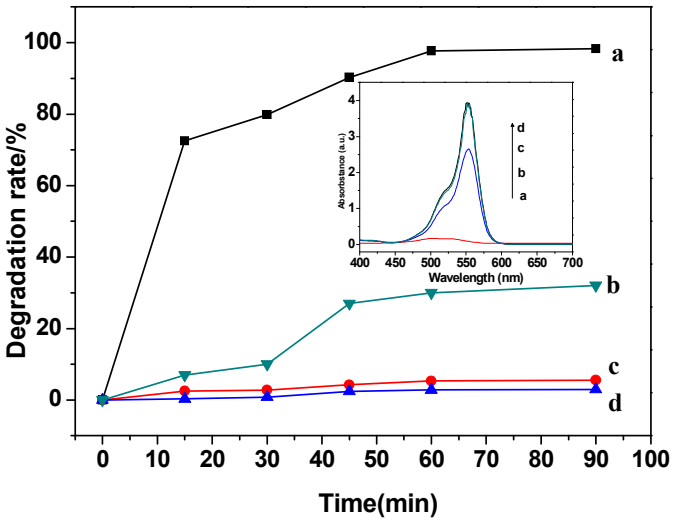

Figure 7